

# Ground-state fidelity and tensor network states for quantum spin tubes

Ai-Min Chen, Qian-Qian Shi, Jin-Hua Liu and Huan-Qiang Zhou<sup>1</sup>

<sup>1</sup>*Centre for Modern Physics and Department of Physics,  
Chongqing University, Chongqing 400044, The People's Republic of China  
(Dated: January 21, 2013)*

An efficient algorithm is developed for quantum spin tubes in the context of the tensor network representations. It allows to efficiently compute the ground-state fidelity per lattice site, which in turn enables us to identify quantum critical points, at which quantum spin tubes undergo quantum phase transitions. As an illustration, we investigate the isosceles spin 1/2 antiferromagnetic three-leg Heisenberg tube. Our simulation results suggest that two Kosterlitz-Thouless transitions occur as the degree of asymmetry of the rung interaction is tuned, thus offering an alternative route towards a resolution to the conflicting results on this issue arising from the density matrix renormalization group.

PACS numbers: 64.60.A-, 05.70.Fh, 75.10.Jm

## I. INTRODUCTION

Recently, significant progress has been made in developing efficient numerical algorithms in the context of the tensor network (TN) representations<sup>1–10</sup>, as a consequence of our deeper understanding of the role of quantum entanglement and fidelity in characterizing critical phenomena in quantum lattice systems. Actually, these developments provide significant insights into the working principle of the density matrix renormalization group (DMRG)<sup>11</sup>, which in turn has led to some novel algorithms based on the TN representations. Among them are the matrix product states (MPS)<sup>1</sup> in one spatial dimension and the projected entangled-pair states (PEPS)<sup>2</sup> in two or higher spatial dimensions. Especially, an infinite MPS (iMPS) algorithm<sup>3</sup> and an infinite PEPS (iPEPS) algorithm<sup>4</sup> have been developed to compute the TN representations of ground-state wave functions for translationally invariant infinite-size quantum systems in one and two or higher spatial dimensions, respectively. A remarkable feature of these TN algorithms is that they offer an efficient way to compute the ground-state fidelity per lattice site<sup>12,13</sup>. Indeed, quantum fidelity allows to capture the ground-state phase diagrams for various quantum lattice systems in condensed matter<sup>12–17</sup>.

There are a class of quantum lattice systems lying between one and two spatial dimensions, namely, quantum spin ladders and tubes. Both experiments and theories<sup>18</sup> have confirmed that the spin 1/2 Heisenberg ladders are gapful for an even number of legs and gapless for an odd number of legs. In fact, the ground state of an odd-leg Heisenberg spin ladder is a gapless spin-liquid or a Tomonaga-Luttinger liquid<sup>19</sup>. Once the periodic boundary conditions are applied in the rung direction, spin ladders become spin tubes. Some exotic phenomena occur due to the geometric frustration for an odd-leg spin tube, which has been realized in some materials, e.g., for three-leg<sup>20</sup> and nine-leg<sup>21</sup> spin tubes. However, little attention has been paid to these systems in the context of the TN representations. Given the importance of both the spin ladders and spin tubes in the theory of strongly correlated systems, it is desirable to develop TN algorithms as an alternative means to investigate their fascinating physics.

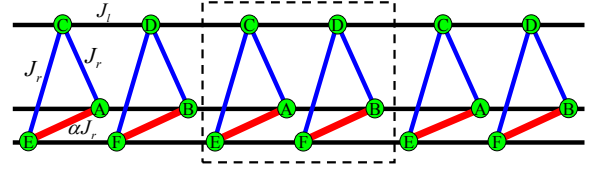


FIG. 1: (Color online) A three-leg spin tube with exchange interaction constants  $J_l$  and  $J_r$  along the leg and rung directions, respectively. Here, an asymmetry parameter  $\alpha$  is introduced as a tunable control parameter. One choice of the unit cell is highlighted in a dash-line box.

This paper is a part of our efforts to develop an efficient numerical algorithm for quantum spin tubes in the context of the TN representations, which offers an efficient way to compute the ground-state fidelity per lattice site. Thus, we are able to locate quantum criticalities for quantum spin tubes. As an illustration, we investigate the isosceles spin 1/2 antiferromagnetic three-leg Heisenberg tube. The simulation results suggest that two Kosterlitz-Thouless (KT) transitions occur as the degree of asymmetry of the rung interaction is tuned.

## II. TENSOR NETWORK STATES FOR QUANTUM SPIN TUBES

Assume that the model Hamiltonian  $H$  describes the nearest-neighbor interaction and is translationally invariant along the leg direction. For a 3-leg spin tube, there are six sites  $A, B, C, D, E$  and  $F$  in each unit cell, as shown in Fig. 1. Such a choice of the unit cell is necessary to accommodate a ground state with spontaneously broken translational symmetry, as it does occur in spin tubes. Indeed, there are two different choices of the unit cell: one is  $ABCDEF$ , as highlighted in Fig. 1, the other is  $BADCFE$ . Any wave function admits a TN representation, which follows from attaching to each site a five-index tensor, as visualized in Fig. 2(a) for a five-index tensor  $A_{lrud}^s$ . Here,  $s$  ( $s = 1, 2, \dots, d$ ) is a physical index from a  $d$ -dimensional local Hilbert space.  $l, r, u$  and  $d$  denote the bond indices from the  $\chi$ -dimensional auxiliary spaces, with  $\chi$  being the truncation dimension, as depicted in Fig. 2(b). In

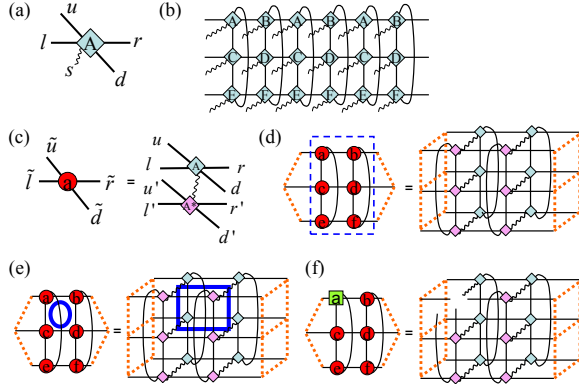


FIG. 2: (Color online) A TN representation for an infinite-size three-leg spin tube. (a) A five-index tensor is attached to each site, with  $l$ ,  $r$ ,  $u$  and  $d$  denoting the inner indices and  $s$  the physical index. (b) A TN representation for a wave function, which is translationally invariant under two-site shifts along the leg direction. (c) An eight-index double tensor  $a_{\tilde{l}\tilde{r}\tilde{u}\tilde{d}}$  is formed, by contracting the physical indices, from the five-index tensor  $A_{lrud}^s$  and its complex conjugate  $A_{l'r'u'd'}^{s*}$ , with  $\tilde{l} \equiv (l, l')$ ,  $\tilde{r} \equiv (r, r')$ ,  $\tilde{u} \equiv (u, u')$ , and  $\tilde{d} \equiv (d, d')$ . (d) The norm  $\langle \psi | \psi \rangle$  of a given wave function in the TN representation. The environment tensors are nothing but the left and right dominant eigenvectors of the transfer matrix consisting of six double tensors. Here, the transfer matrix is highlighted in the dash-line box. (e) The expectation value of a physical observation, such as the four-site Hamiltonian density. (f) The gradient  $\partial \langle \psi | \psi \rangle / \partial A_{lrud}^{s*}$  is equal to the norm with a tensor  $A_{lrud}^{s*}$  absent.

order to measure a physical observable, we define the eight-index double tensors, which are formed, by contracting the physical indices, from the five-index tensors and their complex conjugates, as shown in Fig. 2(c). Fig. 2(d) shows how to compute the norm  $\langle \psi | \psi \rangle$  for a given wave function in the TN representation. Here, a key notion is the transfer matrix, which is highlighted in the dash-line box. The dominant left and right eigenvectors of the transfer matrix are nothing but the environment tensors, in the sense that it accommodates the effect of the remaining part of the infinite-size spin tube system, once the system is partitioned into two parts, with one of them being the transfer matrix. Notice that the norm follows from the dominant eigenvalue  $\lambda_1$  of the transfer matrix.

### III. UPDATING PROCEDURE FOR THE TENSOR NETWORK

We need to update all the tensors in the unit cell during the iteration to generate the ground-state wave function for a given Hamiltonian. Here, we focus on how to update the tensor  $A_{lrud}^s$  to explain the procedure. In fact, other tensors are updated in exactly the same way.

For a given quantum state  $|\psi\rangle$ , the energy per site,  $e$ , is written as

$$E = \lim_{L \rightarrow \infty} \frac{1}{L} \frac{\langle \psi | H | \psi \rangle}{\langle \psi | \psi \rangle}. \quad (1)$$

Here,  $L$  is the total number of the lattice site. In the TN representation, the energy per site,  $e$ , is a functional of the TN tensors, which may be computed efficiently, as shown in Fig. 2(e).

Now we turn to the computation of the gradient of the energy functional with respect to  $A^*$ :

$$G^A = \lim_{L \rightarrow \infty} \frac{1}{L} \left[ \frac{1}{\langle \psi | \psi \rangle} \frac{\partial \langle \psi | H | \psi \rangle}{\partial A^*} - \frac{\langle \psi | H | \psi \rangle}{\langle \psi | \psi \rangle^2} \frac{\partial \langle \psi | \psi \rangle}{\partial A^*} \right], \quad (2)$$

where  $A^*$  is the complex conjugate of  $A$ . Here and hereafter, we have omitted the tensor indices for clarity. In order to compute the energy gradient efficiently, we take advantage of the translational invariance of the Hamiltonian. Since there are two different choices of the unit cell, the contribution to the energy gradient involves six Hamiltonian densities acting on different plaquettes, i.e.,  $h_{ABCD}$ ,  $h_{BADC}$ ,  $h_{CDEF}$ ,  $h_{DCFE}$ ,  $h_{EFAB}$  and  $h_{FEBA}$ . Then the energy gradient becomes

$$G^A = \sum_m G_m^A, \quad (3)$$

with

$$G_m^A = \frac{1}{\langle \psi | \psi \rangle} \frac{\partial \langle \psi | h_m | \psi \rangle}{\partial A^*} - \frac{\langle \psi | h_m | \psi \rangle}{\langle \psi | \psi \rangle^2} \frac{\partial \langle \psi | \psi \rangle}{\partial A^*}. \quad (4)$$

Here,  $h_m \in \{h_{ABCD}, h_{BADC}, h_{CDEF}, h_{DCFE}, h_{EFAB}, h_{FEBA}\}$ . As an example, we take the Hamiltonian density  $h_{ABCD}$  to explain how to compute the gradient. As shown in Fig. 3, there is a TN representation for the gradient  $G_{ABCD}^A$ , in which a hole cell is the cell with the tensor  $A^*$  absent, and a Hamiltonian cell is the cell with the Hamiltonian density  $h_{ABCD}$  sandwiched by attaching to the physical indices between four five-index tensors and their complex conjugates. The expectation value of the Hamiltonian density  $h_{ABCD}$  and the gradient  $\partial \langle \psi | \psi \rangle / \partial A^*$  are shown in Fig. 2(e) and (f), respectively. Notice that the gradient  $\partial \langle \psi | \psi \rangle / \partial A^*$  is nothing but the norm with a tensor  $A^*$  removed. In addition,  $\partial \langle \psi | h_m | \psi \rangle / \partial A^*$  is nothing but the expectation value of  $h_m$  with the tensor  $A^*$  removed. Depending on the relative locations of the hole and the Hamiltonian cells, the TN representation for the energy gradient consists of three parts: (I) the hole and the Hamiltonian density posit on the same cell; (II) the Hamiltonian cell posits on the left hand side of the hole cell; and (III) the Hamiltonian cell posits on the right hand side of the hole cell. It should be emphasized that the gradient decays very fast when the Hamiltonian cell falls apart from the hole cell. That is, only a few Hamiltonian cells need to be taken into account to meet a preset precision. Similarly, one may compute the contribution to the gradient  $G_A$  from other Hamiltonian densities.

Once one knows the energy gradient, the real and imaginary parts,  $A_{re}$  and  $A_{im}$ , of the tensor  $A$  may be updated as follows:

$$\tilde{A}_{re} = A_{re} - \delta \frac{G_{re}^A}{|G_{re}^A|_{\max}}, \quad (5a)$$

$$\tilde{A}_{im} = A_{im} - \delta \frac{G_{im}^A}{|G_{im}^A|_{\max}}, \quad (5b)$$

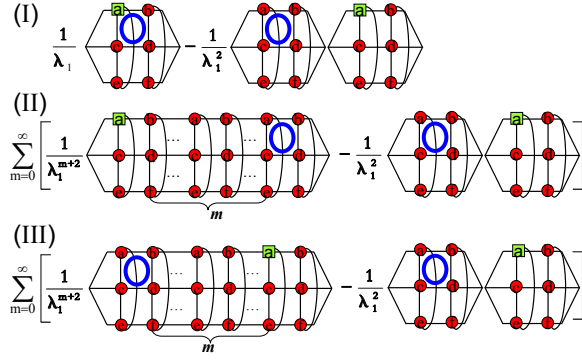


FIG. 3: (Color online) The TN representation for the energy gradient  $G^A$  with respect to the tensor  $A^*$ . A small circle represents a double tensor attached to each site, a square indicates the absence of the tensor  $A^*$ , and a large circle is the Hamiltonian density acting on a plaquette in the unit cell. Here,  $\lambda_1$  denotes the dominant eigenvalue of the transfer matrix. The TN for the energy gradient consists of three parts: (I) the hole and the Hamiltonian density posit on the same cell; (II) and (III) the Hamiltonian cell posits on the left and right hand sides of the hole cell, respectively. Here,  $m$  is the cell number between the hole cell and the Hamiltonian cell. Notice that only the contribution from the plaquette Hamiltonian density  $h_{ABCD}$  is shown.

where  $G_{re}^A$  and  $G_{im}^A$  are, respectively, the real and imaginary parts of the five-index tensors  $G^A$ ,  $\delta$  is the step size for an update. During the implementation, it is tuned to be decreasing with the number of the iteration steps. Notice that both the sign and magnitude of the energy gradients  $G_{re}^A$  and  $G_{im}^A$  are exploited. As such, the tensor  $A$  is updated to  $\tilde{A} = \tilde{A}_{re} + i\tilde{A}_{im}$ . Actually, all the six tensors in the unit cell are updated simultaneously. Repeating the procedure until the ground-state energy per site converges, an approximate ground-state wave function is generated in the TN representation.

#### IV. MODEL

We consider the antiferromagnetic spin 1/2 three-leg Heisenberg tube, as depicted in Fig. 1, on an infinite-size lattice. The Hamiltonian takes the form

$$\hat{H} = \hat{H}_{\text{leg}} + \hat{H}_{\text{rung}}, \quad (6a)$$

$$\hat{H}_{\text{leg}} = J_l \sum_{i,j} \mathbf{S}_{i,j} \cdot \mathbf{S}_{i+1,j}, \quad (6b)$$

$$\hat{H}_{\text{rung}} = J_r \sum_i (\mathbf{S}_{i,1} \cdot \mathbf{S}_{i,2} + \mathbf{S}_{i,2} \cdot \mathbf{S}_{i,3} + \alpha \mathbf{S}_{i,3} \cdot \mathbf{S}_{i,1}), \quad (6c)$$

where  $\mathbf{S}_{i,j}$  is the spin-1/2 Pauli operators at leg  $i$  and rung  $j$  ( $j = 1, 2, 3$ ),  $J_l$  is the neighboring exchange interaction along the legs and  $J_r$  stands for the rung interaction. For the antiferromagnetic coupling, the model is frustrated along the rung direction. The asymmetric parameter  $\alpha$  controls the strength of the frustration. If the asymmetric parameter  $\alpha$  is varied, the

model exhibits two limiting cases: for  $\alpha = 0$ , it corresponds to the three-leg ladder; for  $\alpha \rightarrow \infty$ , it becomes a decoupled system consisting of a single chain and a two-leg ladder. Both of them are gapless Tomonaga-Luttinger liquids, with the central charge  $c = 1$ , and possess the  $SU(2)$  symmetry. When  $\alpha = 1$ , the system is spontaneously dimerized, arising from the geometric frustration. All the spin excitations are gapful, as follows from the Lieb-Schultz-Mattis theorem<sup>22</sup>: two degenerate ground states arise from the broken translational symmetry. Therefore, one may expect that at least one phase transition point occurs if the asymmetric parameter  $\alpha$  is tuned from 0 to  $\infty$ . From now on, we fix  $J_l$  and  $J_r$  to be unity, and focus on the effect of the asymmetry of the rung interaction.

Previous studies for this model based on the DMRG simulations leads to somewhat controversial results: Nishimoto and Arikawa suggested that the spin gap vanishes as soon as the infinitesimally small asymmetry is introduced<sup>23</sup>, while Sakai *et. el.*<sup>24</sup> argued that a finite spin gap appears in a narrow region around the rung-symmetry line and the phase transitions between the gapless and gapful phases belong to the KT universality class.

#### V. NUMERICAL SIMULATION

For a quantum system described by the Hamiltonian  $H(\alpha)$ , with  $\alpha$  being the control parameter, the fidelity  $F(\alpha_1, \alpha_2) \equiv |\langle \Psi(\alpha_2) | \Psi(\alpha_1) \rangle|$  between two ground states  $|\Psi(\alpha_1)\rangle$  and  $|\Psi(\alpha_2)\rangle$  scales as  $F(\alpha_1, \alpha_2) \sim d(\alpha_1, \alpha_2)^L$ . Here,  $d(\alpha_1, \alpha_2)$  is the ground-state fidelity per lattice site, which characterizes how fast changes when the thermodynamic limit is approached<sup>12,13</sup>. It satisfies the properties inherited from the fidelity  $F(\alpha_1, \alpha_2)$ : (i) normalization  $d(\alpha, \alpha) = 1$ ; (ii) symmetry  $d(\alpha_1, \alpha_2) = d(\alpha_2, \alpha_1)$ ; and (iii) range  $0 \leq d(\alpha_1, \alpha_2) \leq 1$ . The ground-state fidelity per lattice site exhibits singularities as a pinch point when the control parameter  $\alpha$  crosses a transition point  $\alpha_c$ .

The TN algorithm for quantum spin tubes, as described, allows to efficiently compute the ground-state fidelity per lattice site. In Fig. 4, the ground-state fidelity per lattice site,  $d(\alpha_1, \alpha_2)$ , is plotted for the spin 1/2 three-leg Heisenberg tube, with truncation dimension  $\chi = 6$ . Two transition points are identified, as two pinch points on the fidelity surface clearly indicates that there are two phase transitions at  $\alpha_{c1} \sim 0.95$  and  $\alpha_{c2} \sim 1.06$ , respectively. Between two phase transition points, a finite gap opens, which follows from the Lieb-Schultz-Mattis theorem, due to spontaneous symmetry breaking of the translational symmetry, as reflected in the two-site reduced density matrices. Given that both gapless phases are Tomonaga-Luttinger liquids (see below for a detailed discussion), the phase transitions between the gapless and gapful phases belong to the KT universality class. Our results support the DMRG results by Sakai *et. el.*<sup>24</sup>.

In Fig. 5, we plot the ground-state fidelity per lattice site,  $d(\alpha_1, \alpha_2)$ , as a function of  $\alpha_1$ , for a fixed  $\alpha_2$ , with different truncation dimensions  $\chi$ . Here, two reference states  $\Psi(\alpha_2 = 0)$  and  $\Psi(\alpha_2 = 2)$  in the pseudo- $SU(2)$ -symmetry-broken phases have been chosen, respectively<sup>25</sup>. The simulation is per-

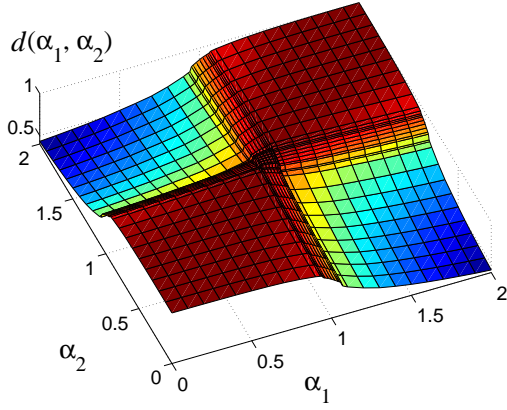


FIG. 4: (Color online) The ground-state fidelity per lattice site,  $d(\alpha_1, \alpha_2)$ , for the spin 1/2 three-leg Heisenberg tube with truncation dimension  $\chi = 6$ . The fidelity surface clearly indicates that there are two transition points, as two pinch points occur at  $\alpha_{c1} \sim 0.95$  and  $\alpha_{c2} \sim 1.06$ , respectively.

formed for a randomly chosen initial state. The algorithm automatically produces degenerate ground states which pseudo-break the  $SU(2)$  symmetry in the Tomonaga-Luttinger liquid phases. In the pseudo-symmetry-broken phase, the ground-state fidelity per lattice site,  $d(\alpha_1, \alpha_2)$ , exhibits different values lying between two (extreme) degenerate ground states. In the symmetric phase,  $d(\alpha_1, \alpha_2)$  yields just one value. Thus, a bifurcation point occurs, which coincides with the transition point  $\alpha_c$ . Therefore, two phase transition points at  $\alpha_{c1} \sim 0.95$  and  $\alpha_{c2} \sim 1.06$  are identified from the bifurcation in the ground-state fidelity per lattice site. A smoking-gun signature of the Tomonaga-Luttinger liquids is that such a bifurcation tends to disappear when the truncation dimension  $\chi$  goes to infinity<sup>25</sup>, as required to keep consistent with the Mermin-Wagner theorem<sup>26</sup> that no continuous symmetry is spontaneously broken in a one-dimensional quantum system. This implies that the degenerate ground states arise from the finiteness of the truncation dimension, an artifact of the algorithm. However, the singularity associated with the bifurcation still remains (as an essential singularity as it should be for the KT transitions), even if the truncation dimension goes to infinity. Notice that the Goldstone modes survive as gapless excitations in the limiting case without truncation.

## VI. CONCLUSION

In this paper, an efficient algorithm has been developed for quantum spin tubes in the context of the TN representations. It

allows to efficiently compute the fidelity per lattice site, which enables us to identify quantum criticalities for quantum spin tubes. Our simulation results for the isosceles spin 1/2 anti-ferromagnetic three-leg Heisenberg tube suggest that two KT transitions occur as the degree of asymmetry of the rung interaction is tuned, thus offering an alternative route towards a resolution to the conflicting results on this issue arising from

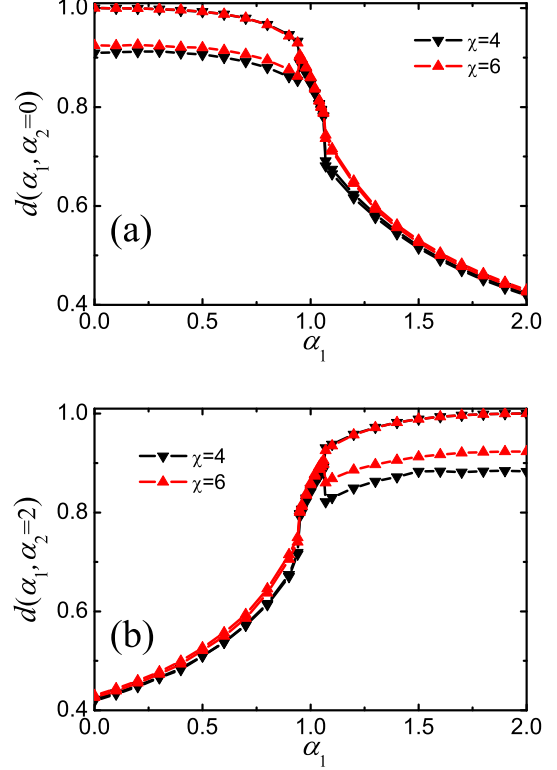


FIG. 5: (Color online) The ground-state fidelity per lattice site,  $d(\alpha_1, \alpha_2)$ , as a function of  $\alpha_1$  for a fixed  $\alpha_2$ . The truncation dimension is fixed as  $\chi = 4$  and  $\chi = 6$ , respectively. Here, the reference state has been chosen: (a)  $\Psi(\alpha_2 = 0)$  and (b)  $\Psi(\alpha_2 = 2)$ .

the DMRG simulations.

## Acknowledgements

The work is supported by the National Natural Science Foundation of China (Grant No: 10874252) and the Fundamental Research Funds for Central Universities (Project No. CDJXS11102213).

<sup>1</sup> M. Fannes, B. Nachtergaele, and R. F. Werner, *Comm. Math. Phys.*, **144**, 443 (1992); S. Östlund and S. Rommer, *Phys. Rev. Lett.*, **75**, 3537 (1995).

<sup>2</sup> F. Verstraete and J. I. Cirac, *arXiv: cond-mat/0407066*.

<sup>3</sup> G. Vidal, *Phys. Rev. Lett.*, **98**, 070201 (2007).

<sup>4</sup> J. Jordan, R. Orus, G. Vidal, F. Verstraete and J. I. Cirac, *Phys.*

- Rev. Lett. **101**, 250602 (2008).
- <sup>5</sup> P. Pippin, S. R. White, and H. G. Evertz, Phys. Rev. B **81**, 081103(R) (2010).
  - <sup>6</sup> Q.-Q. Shi and H.-Q. Zhou, J. Phys. A: Math. Theor. **42**, 272002 (2009).
  - <sup>7</sup> B. Pirvu, F. Verstraete, and G. Vidal, Phys. Rev. B **83**, 125104 (2011).
  - <sup>8</sup> J. Haegeman, J. I. Cirac, T. J. Osborne, I. Pižorn, H. Verschelde, and F. Verstraete, arXiv:1103.0936.
  - <sup>9</sup> H. C. Jiang, Z. Y. Weng, and T. Xiang, Phys. Rev. Lett. **101**, 090603 (2008).
  - <sup>10</sup> L. Wang, Y.-J. Kao, and A.W. Sandvik, Phys. Rev. E **83**, 056703 (2011).
  - <sup>11</sup> S. R. White, Phys. Rev. Lett. **69**, 2863 (1992); S. R. White, Phys. Rev. B **48**, 10345 (1993); U. Schollwoeck, Rev. Mod. Phys. **77**, 259 (2005).
  - <sup>12</sup> H.-Q. Zhou and J. P. Barjaktarevič, J. Phys. A: Math. Theor. **41**, 412001 (2008); H.-Q. Zhou, J.-H. Zhao, and B. Li, J. Phys. A: Math. Theor. **41**, 492002 (2008); H.-Q. Zhou, e-print arXiv: 0704.2945.
  - <sup>13</sup> H.-Q. Zhou, R. Orús, and G. Vidal, Phys. Rev. Lett. **100**, 080601 (2008).
  - <sup>14</sup> M.M. Rams and B. Damski, Phys. Rev. Lett. **106**, 055701 (2011).
  - <sup>15</sup> P. Zanardi, M. Cozzini, and P. Giorda, J. Stat. Mech. L02002, (2007); N. Oelkers and J. Links, Phys. Rev. B **75**, 115119 (2007); M. Cozzini, R. Ionicioiu, and P. Zanardi, Phys. Rev. B **76**, 104420 (2007); L. Campos Venuti and P. Zanardi, Phys. Rev. Lett. **99**, 095701 (2007).
  - <sup>16</sup> W.-L. You, Y.-W. Li, and S.-J. Gu, Phys. Rev. E **76**, 022101 (2007); S. J. Gu, H. M. Kwok, W. Q. Ning, and H. Q. Lin, Phys. Rev. B **77**, 245109 (2008); M. F. Yang, Phys. Rev. B **76**, 180403(R) (2007); Y. C. Tzeng and M. F. Yang, Phys. Rev. A **77**, 012311 (2008); J. O. Fjærestad, J. Stat. Mech.: Theory Exp. (2008) P07011; T. Liu, Y.-Y. Zhang, Q.-H. Chen, and K.-L. Wang, Phys. Rev. A **80**, 023810 (2009); J. Sirker, Phys. Rev. Lett. **105**, 117203 (2010).
  - <sup>17</sup> S. Chen, L. Wang, Y. Hao, and Y. Wang, Phys. Rev. A **77**, 032111 (2008); S. Chen, L. Wang, S.-J. Gu, and Y. Wang, Phys. Rev. E **76**, 061108 (2007).
  - <sup>18</sup> E. Dagotto and T. M. Rice, Science **271**, 618 (1996); E. Dagotto, Rep. Prog. Phys. **62**, 1525 (1999).
  - <sup>19</sup> T. Giamarchi, *Quantum Physics in One Dimension* (Oxford University Press, Oxford, 2004).
  - <sup>20</sup> J. Schnack, H. Nojiri, P. Kögerler, G. J. T. Cooper, and L. Cronin, Phys. Rev. B **70**, 174420 (2004); G. Seeber, P. Kögerler, B. M. Kariuki, and L. Cronin, Chem. Commun. (Cambridge) **2004**, 1580 (2004).
  - <sup>21</sup> P. Millet, J. Y. Henry, F. Mila, and J. Galy, J. Solid State Chem. **147**, 676 (1999); J. L. Gavilano, D. Rau, S. Mushkolaj, H. R. Ott, P. Millet, and F. Mila, Phys. Rev. Lett. **90**, 167202 (2003).
  - <sup>22</sup> E. Lieb, T. Schultz, and D. Mattis, Ann. Phys. (New York) **16**, 407 (1961).
  - <sup>23</sup> S. Nishimoto and M. Arikawa, Phys. Rev. B **78**, 054421 (2008).
  - <sup>24</sup> T. Sakai, M. Sato, K. Okunishi, Y. Otsuka, K. Okamoto, and C. Itoi, Phys. Rev. B **78**, 184415 (2008).
  - <sup>25</sup> H.-L. Wang, J.-H. Zhao, B. Li, and H.-Q. Zhou, arXiv:0902.1670.
  - <sup>26</sup> N. D. Mermin and H. Wagner, Phys. Rev. Lett. **17**, 1133 (1966).